ON THE PERFORMANCE OF TWO ADVANCED LAND SURFACE SCHEMES AS APPLIED TO SIMULATIONS OF ARCTIC LAND ENVIRONMENTS

Ipshita Majhi, Jing Zhang, Jeffrey S. Tilley, and Nicole Mölders

Geophysical Institute, University of Alaska Fairbanks, Fairbanks AK

1. Introduction

The partitioning of precipitation reaching the earth's surface among evaporation, transpiration, infiltration, and runoff is mainly governed by the highly non-linear exchange between the soil, vegetation and atmosphere. Surface-atmosphere interaction can be important for not only the disposition of the precipitated water, but also to where precipitation falls in the first place. Thus, there are strong efforts to improve mesoscale meteorological models by introducing state-of-the-art land surface models (LSMs; e.g., Tilley and Lynch 1998, Chen and Dudhia 2001a, b, Mölders 2000). Such LSMs describe the important interactions between the biosphere and atmosphere, especially, the fluxes of radiation, momentum, heat and matter.

The comparisons carried out within the framework of the Intercomparison of Land Parameterization Schemes (PILPS) program showed that even quite similarly designed LSMs may provide appreciable differences in the results (e.g., Shao and Henderson-Sellers 1996, Chen et al. 1997). One conclusion of this study was that systematic comparison of LSMs and their results may lead to a better understanding of nature of these differences and may lead to improved process representation. This is the goal of the present study.

We compare and evaluate the performance of two state-of-the-art LSMs, namely, the NCEP Oregon State University Air Force Hydrology Lab land surface model (NOAH ; e.g., Koren et al, 1999) with its modifications made for the Arctic (e.g.,, Mitchell et al. 2002) and the hydro-thermodynamic soil vegetation scheme (HTSVS; Kramm et al. 1994, 1996, Mölders 2000, Mölders et al. 2003a). Hereafter, the LSMs are denoted NOAH and HTSVS, respectively, as are the simulations performed with these LSMs and their results. NOAH and HTSVS were chosen for the following reasons: (1) both LSMs have been evaluated initially with different data sets (e.g., Kramm 1995, Kramm et al. 1996, Mölders 2000, Mölders et al. 2003a, b, Chen and Dudhia 2001a, b, Zhang and Tilley 2003 (this volume)), (2) they were developed for different regions and purposes of application, (3) both LSMs are commonly applied in the scientific community.

The predecessor to NOAH, the Oregon State LSM (e.g., Ek and Mahrt 1991) was designed for short to medium range meteorological forecasts. On this temporal scale the Ludwig-Soret (i.e., a temperature gradient contributes to the water flux and changes soil volumetric water content) and Dufor (i.e., a moisture gradient contributes to the heat flux and alters soil temperature) effects and the differences between foliage and ground temperature are assumed to be negligible. This prior version was evaluated in a 1D-mode against FIFE, HAPEX-MOBILHY, and CABAUW-data. It reasonably simulates the diurnal variation and seasonal evolution of surface heat fluxes, surface radiative temperature, and soil moisture (Chen et al. 1996). Its incorporation in the Eta-model significantly improved the quantitative precipitation forecast skill (Chen et al. 1997). The land surface model was further-developed for application in high-latitudes (e.g., Koren et al. 1999, Zhang and Tilley 2001, Mitchell et al. 2002) and evaluated for various Arctic sites (Zhang and Tilley 2003, this volume).

HTSVS originally was developed for chemistry (CM) and chemistry transport (CTM) models and long-term climate simulations (e.g., Kramm et al. 1994, 1996, Mölders et al. 2003a). In CMs and CTMs, the emission of trace species from and its transport within the soil are important issues, for which water vapor transport in the soil and the Ludwig-Soret effect and Dufour effect are considered. These effects are also of relevance for the long-term variability of soil water and within permafrost. HTSVS considers the heterogeneity on the microscale, which is of relevance on the climate scale. The heterogeneity on the microscale is considered by determining separate moisture and temperature values for the foliage and ground by a mixture approach (Fig. 1).

Several off-line evaluation studies were performed with HTSVS over various vegetation types using data from GREIV-74 (Kramm 1995), SANA, and Jülich-experiment (Kramm et al. 1996) as well as CASES97 (Mölders 2000). A long-term evaluation was carried out using the lysimeter and tensiometer data collected at Brandis, Germany during 1992 to 1997 (Mölders et al. 2003). These studies have demonstrated that HTSVS reasonably simulates the diurnal variation of soil temperatures, surface latent and sensible heat fluxes as well as the seasonal evolution of water tension and subsurface runoff.

2. Design of the study

In this study we will first theoretically analyze the different and common features of the two land surface models before we evaluate their results. In the context of this article we primarily discuss the parameterizations as well as the parameters used by the models and provide some estimates to evaluate what the differences mean. Presentation of more detailed simulation comparisons will be done at the conference.

Routine hourly mean data for wind, relative humidity, temperature, global radiation, and precipitation are continuously available for several sites in Alaska. We use these data to drive the land-surface models. For some sites, no data of downward long-wave radiation are available; this quantity will be parameterized at such sites. Data of observed soil temperatures, soil moisture and snow depth serve for evaluation of the models.

We anticipate that the primary differences between the models will be in the soil moisture and temperature fields, skin surface temperatures as well as sensible and latent heat fluxes. Secondary differences are expected for the variables of state. .

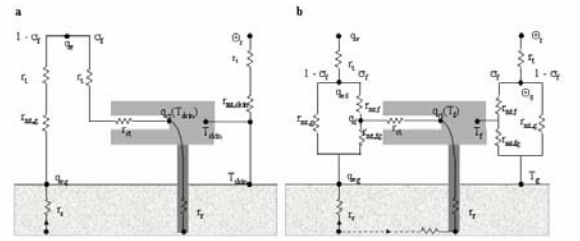

Fig. 1. Schematic view of the resistance networks used in (a) NOAH-LSM and (b) HTSVS. Here, r_r, r_t, $r_{mt,fg}$, $r_{mt,g}$, $r_{mt,f}$, and $r_{mt,skin}$ are the resistance of roots, turbulent resistance, molecular turbulent resistance between ground and foliage, for ground, foliage, as well as for the skin consisting of ground and foliage, q_v, q_{vg}, q_{st}, q_f, Θ_r, T_g, T_f, T_{skin}, and σ_f stand for the specific humidity at reference height and at the ground, specific humidity in the stomata (saturation) and of the foliage, potential temperature at reference height, temperatures of the ground, foliage, and skin, respectively, as well as vegetation fraction.

3. Results from theoretical analysis of NOAH and HTSVS

3.1 Prognostic equations and numerical treatment

In NOAH, prognostic variables are soil moisture and soil temperature each in four layers, water stored on the canopy and snow depth at the ground surface, respectively. In HTSVS, the prognostic variables are the volumetric water content and soil temperature each in five layers, the water and snow stored on the entire surface (soil and canopy), snow liquid water content, snow density, and snow temperature. Note that in principle, more soil layers can be chosen in HTSVS and NOAH. Here, however, we take the design as it is implemented in MM5 (e.g., Chen and Dudhia 2001, Mölders 2000).

3.2 Discretization of the soil

In principle, soil layers can be chosen arbitrarily in NOAH. In HTSVS, for numerical reasons, the soil is divided into layers according to $\Delta\xi = \ln(z_{i+1}/z_i) =$ constant where z_{i+1} and z_i are neighboring soil layers with $z_{i+1} > z_i$.

3.3 Soil volumetric heat capacity

In both LSMs, the dependence of the volumetric heat capacity of moist soil, C, on soil volumetric water content is considered by

$$C=(1-\eta_s)\rho_S c_S+\eta\rho_w c_w+\eta_i\rho_i c_i+(\eta_s-\eta-\eta_i)\rho_a c_p \quad . \quad (1)$$

Here, η_s is the porosity (Tables 1, 2), ρ_S, ρ_w (= 1000 kg/m^3), ρ_i (= 916 kg/m^3), and ρ_a are the density of dry soil, water, ice, and air. Furthermore, c_S, c_w, c_i, and c_a denote the specific soil heat capacity, specific heat of water, ice, and air, respectively.

In NOAH, volumetric heat capacity of dry soil material is equal to $2\cdot10^6$ Wm^{-3}K^{-1}s^{-1} while the density of the dry soil material is given by

$$\rho_S = (1-\eta_s)2700 \quad . \quad (2)$$

Using these relations yields the volumetric heat capacity used in NOAH. The volumetric heat capacity of dry soil material, $\rho_S c_S$, as used in HTSVS, is listed in Table 2.

The resulting different values for volumetric heat capacity of the soils are different in NOAH and HTSVS and, hence will lead to a different thermal behavior. Assuming, for example, a volumetric water content of 0.3 for sand and a density of air of 1.29 kg/m^3, we obtain a volumetric heat capacity values for wet soil of about $2.228\cdot10^6$ Wm^{-3}K^{-1}s^{-1} and $2.796\cdot10^6$ Wm^{-3}K^{-1}s^{-1} for HTSVS and NOAH, respectively.

3.4 Soil hydraulic conductivity

In both LSMs, the hydraulic conductivity is given by (e.g., Clapp and Hornberger 1978)

$$K_w = K_{ws}\,(\eta/\eta_s)^{2b+3} \quad . \quad (3)$$

In HTSVS, the soil characteristic curve is described by

$$P_f = 2 + \log_{10}(-\Psi_s(\eta_s/\eta)^b) \qquad (4)$$

where the water potential, Ψ, is determined by (e.g., Clapp and Hornberger 1978)

$$\Psi = \Psi_s\left(\frac{\eta}{\eta_s}\right)^{-b} \quad , \qquad (5)$$

with ψ_s being the soil water potential at saturation (see Tab. 2).

The water tension, Ψ', used in NOAH can be related to the water potential of HTSVS by multiplication with -1 (see also Tabs. 1, 2).

3.5 Soil thermal conductivity

In both LSMs, thermal conductivity is a function of soil volumetric water (and in the case of frozen soil of soil volumetric ice content). However, the formulation differs between the models. In NOAH, the thermal conductivity is given as

$$\lambda = A(\lambda_s - \lambda_d) + \lambda_d \quad . \qquad (6)$$

where

$$A = \begin{cases} \eta/\eta_s & \text{frozen soil} \\ \log_{10}\eta/\eta_s + 1 & \text{unfrozen soil} \\ 0 & \text{dry soil} \end{cases} \qquad (7)$$

and

$$\lambda_d = \frac{(0.135(1-\eta_s)2700 + 64.7)}{(2700 - 0.94)(1-\eta_s)2700} \qquad (8)$$

and

$$\lambda_s = \left(\lambda_{qz}^{qz}\lambda_0^{1-qz}\right)^{1-\eta_s}\lambda_i^{\eta_i}\lambda_w^{\eta} \quad . \qquad (9)$$

Here, λ_i and λ_w are the thermal conductivity of ice and water, respectively. Furthermore, λ_{qz} and λ_0 stand for the thermal conductivity of quartz and other dry soil material.

In HTSVS, the thermal conductivity λ depends on this quantity as follows (e.g., McCumber and Pielke 1981)

$$\lambda = \begin{cases} 419\exp(-2.7 + P_f))\, 0 < P_f \le 5.1 \\ 0.172 \;\; P_f > 5.1 \end{cases} \qquad (10)$$

In the case of frozen soil, a mass-weighted thermal conductivity depending on the liquid and solid volumetric water content present is calculated in HTSVS using the above equation for the liquid phase and a value of 2.31 J/(msK) for the solid phase.

3. 6 Soil moisture and heat fluxes

Both LSMs use a fully implicit Crank-Nicholson-scheme for soil moisture and temperature prediction.

3.6.1 NOAH

In NOAH, the soil heat flux is determined by a diffusion equation for soil temperature, T_S (e.g., Chen et al. 1996)

$$C\frac{\partial T_S}{\partial t} = \frac{\partial}{\partial z}\left(\lambda\frac{\partial T_S}{\partial z}\right) \quad , \qquad (11)$$

where t is time, λ is the thermal conductivity, z is soil depth, and C is the volumetric heat capacity of the moist soil. At the top, ground heat flux is determined using the surface skin temperature. Volumetric water content is given by the diffusive form of Richard's equation derived from Darcy's law under the assumption of rigid, homogeneous, isotropic vertical flow conditions (e.g., Chen et al. 1996)

$$\frac{\partial\eta}{\partial t} = \frac{\partial}{\partial z}\left(D\frac{\partial\eta}{\partial z}\right) + \frac{\partial K_w}{\partial z} \quad . \qquad (12)$$

Here, η is the volumetric liquid water content, K_w is the hydraulic conductivity and the hydraulic diffusivity of frozen soil is given by

$$D = F\cdot D_s\left(\frac{\eta_t}{\eta_s}\right)^{b+2} + (1-F)D_s\left(\frac{0.2}{\eta_s}\right)^{b+2} \qquad (13)$$

with

$$F = \frac{1}{1 + (500.\eta_i)^3} \quad . \qquad (14)$$

where η_i is the ice content within the soil layer, and η_t is the total soil moisture (ice plus liquid) within the soil layer, D_s is the saturated soil diffusivity, and

η_s is the soil porosity. In NOAH, ice formation is adjusted to the energy loss of a soil layer at temperatures below the freezing point. Thus, the soil ice content of the next time step (t=n+1) is given by

$$\eta_i^{n+1} = \eta_i^n + \frac{\alpha \Delta t}{3.35 \cdot 10^8 \Delta z} \qquad (15)$$

where Δz, Δt, and α are the thickness of the soil layer, the time step and the heat flux, respectively. The ice content is a function of soil texture and soil temperature (see Koren et al. 1999)

$$\frac{g\Psi_s}{L_f}\left(1-c_k\eta_i\right)^2\left(\frac{\eta-\eta_i}{\eta_s}\right)^{-b} + \frac{T}{T+273.16} = 0 \quad . \qquad (16)$$

3.6.2 HTSVS

In HTSVS, the treatment of the (vertical) heat- and water-transfer processes is based on the principles of the linear thermodynamics of irreversible processes including the Richards-equation. Since the seasonally frozen soil affects the surface energy balance and the hydrologic response, a diagnostic approach to consider the effects of frozen soil was added to the diffusion equations for soil moisture and heat. The governing balance equations for heat and moisture including phase transition processes and water extraction by roots read (Mölders et al. 2003a)

$$C\frac{\partial T_S}{\partial t} = -\frac{\partial}{\partial z_S}\left(-\left(\lambda+L_v\rho_w D_{T,v}\right)\frac{\partial T_S}{\partial z_S} - L_v\rho_w D_{\eta,v}\frac{\partial \eta}{\partial z_S}\right) + L_f\rho_i\frac{\partial \eta_i}{\partial t} \qquad (17)$$

and

$$\frac{\partial \eta}{\partial t} = \frac{\partial}{\partial z_S}\left(\left(D_{\eta,v}+D_{\eta,w}\right)\frac{\partial \eta}{\partial z_S} + D_{T,v}\frac{\partial T_S}{\partial z_S} + K_w\right) - \frac{\chi}{\rho_w} - \frac{\rho_i}{\rho_w}\frac{\partial \eta_i}{\partial t} \qquad (18)$$

The second terms on the right hand side of the last two equations represent the Ludwig-Soret effect and the Dufor effect. The third term in the last equation stands for the water uptake by roots, χ/ρ_w. This coupled equation system is simultaneously solved by using the Crank-Nicholson-scheme in conjunction with the Gauss-Seidel-technique. The transfer coefficients for water vapor, $D_{\eta,v}$, water, $D_{\eta,w}$, and heat, $D_{T,v}$, depend on the relative volumetric water content, η/η_s according to (e.g., de Vries 1958, Kramm et al. 1996, Mölders 1999)

$$D_{T,v} = D_v\eta_s\left(1-\frac{\eta}{\eta_s}\right)\frac{\rho_v}{\rho_w}\frac{L_v - g\Psi}{R_v T_S^2} \qquad (19)$$

$$D_{\eta,v} = D_v b\left(1-\left(\frac{\eta}{\eta_s}\right)^{-1}\right)\frac{\rho_v}{\rho_w}\frac{g\Psi}{R_v T_S} \qquad (20)$$

$$D_{\eta,w} = -bK_{w,s}\frac{\Psi_s}{\eta_s}\left(\frac{\eta}{\eta_s}\right)^{b+3} \quad . \qquad (21)$$

Here, g is the acceleration of gravity, Ψ stands for the water potential (also called matric potential, soil water suction and tension head), L_v is the latent heat of condensation, L_f is the latent heat of fusion, R_v and ρ_v are the gas constant and density of water vapor. The values of the pore-size distribution index, b, and hydraulic conductivity, $K_{w,s}$, depend on soil type. The molecular diffusion coefficient of water vapor in air is given by (Kramm 1995)

$$D_v = \alpha_T\frac{5.89\cdot 10^{-8}T^{2.3}}{p} \qquad (22)$$

where p is pressure (in hPa), and $\alpha_T = 0.67$ is a factor to consider the torsion of soil by roots and worms.

In HTSVS, in the presence of ice, water potential remains in local equilibrium with the vapor pressure over pure ice (e.g., Fuchs et al. 1978)

$$\psi = \frac{L_f\left(T_S - 273.15\right)}{gT_S} \quad . \qquad (23)$$

The volumetric ice content is defined by the difference of the total water within the soil layer minus the maximum liquid water content for temperatures below the freezing point, T_0:

$$\eta_{max} = \eta_s\left\{\frac{L_f\left(T_S - T_0\right)}{g\psi_s T_S}\right\}^{-1/b} \quad . \qquad (24)$$

Since the phase-transition alters temperature by release of latent heat or consumption of heat, a first-order Newton-Ralphson-technique is used to solve the moisture and heat flux equations iteratively in HTSVS.

Since the most obvious differences between NOAH and HTSVS are the cross-effects (thermal and moisture) that are only included in the latter, we examined the impact of these cross-effects. Figure 2 shows the results from simulations performed with

HTSVS wherein soil moisture is taken from different levels in the soil. The resulting distribution of η leads to altered gradients of that quantity and, hence, altered soil moisture and heat fluxes as well as soil temperatures. It is noteworthy that the cross-effects affect the long term (2050-day-sums) of recharge and water supply to the atmosphere by about 5 % each (cf. Mölders et al. 2003a). From this we conclude that cross-effects are important on the long-term, but can be neglected on the shorter time scales (days to weeks) as it is the case for NOAH.

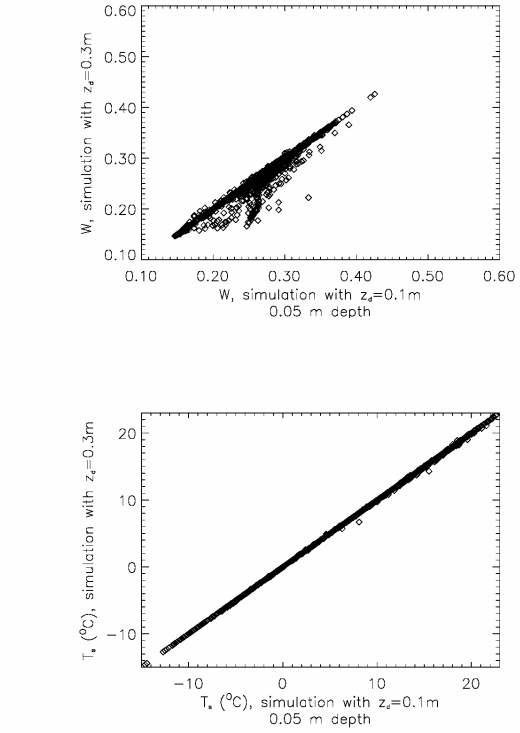

Fig. 2. Comparison of daily averaged (a) soil volumetric water content and (b) soil temperature as obtained from the simulations for 2050 days with HTSVS assuming 0.1 m and 0.3 as the depths for the partitioning between the upper and lower root zone. The scatter in soil temperatures provides a hint for how the Dufour- and Ludwig-Soret effects work on the long-term. See text for further discussion. After Mölders et al. (2003a).

3.7. Exchange of heat and matter at the interface land-atmosphere

In both LSMs, vegetation is represented by a single canopy layer. The sources and sinks of soil moisture are infiltration, *I*, evapotranspiration, *E*, surface runoff, *R*, and base flow, *B*, (drainage). The exchange of energy and matter between the vegetation/soil and the atmosphere is parameterized by a resistance network analogy (Fig. 1). Transpiration of water by plants is described by a bulk-stomatal resistance approach (see Ek and Mahrt 1991, Chen et al. 1996 for NOAH, and Kramm et al. 1996 for HTSVS, respectively). Despite accounting for the same processes, different strategies are applied to calculate the exchange of heat and matter as can be seen by comparison of Figures 1 and 3.

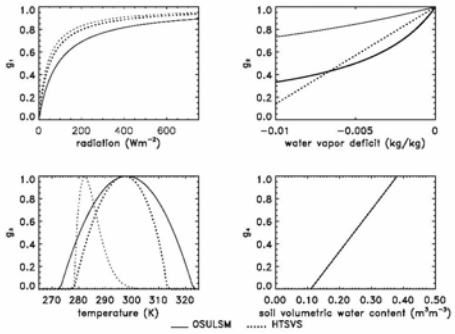

Fig. 3. Comparison of correction functions as used for the case simulated by NOAH (solid lines) and HTSVS (dotted lines) for the effects of temperature, water vapor deficit, radiation and soil volumetric water content (from the upper left to the lower right). In HTSVS, correction functions of radiation and temperature depend on vegetation type. Here, they are shown for grassland (thin dotted lines) and cropland (thick dotted lines). In NOAH-LSM, sensitivity to water vapor deficit is plant specific. Here, grassland (thin solid lines) and forest (thick solid lines) are shown.

Stomatal resistance,

$$r_{st} = \frac{r_{st,\min}}{g_1 g_2 g_3 g_4} \quad , \qquad (25)$$

depends on the sensitivity of transpiration to photosynthetic active radiation, temperature, water vapor deficit between leaf and ambient air. These stress factors are accounted for by correction functions, g_1 to g_4, which range between 0 and 1 (e.g., Jarvis 1976; Fig. 3; Tab. 4). The correction functions of NOAH were adjusted for mesoscale applications using FIFE-data (Chen et al. 1996).

Below a critical value solar radiation strongly affects stomatal resistance (Fig. 3). This critical value is higher for NOAH than for HTSVS because the latter model was developed for higher latitude applications (initially) than the former. Consequently, cloudiness, sunrise and sunset may affect transpiration more strongly in NOAH than in HTSVS.

When the water vapor deficit is high, plants close stomata to protect themselves from water loss. In NOAH, this effect depends on land-use type (cf. Tabs. 2, 4, 5). According to the correction functions, a water vapor deficit increases stomatal resistance more strongly in HTSVS than in NOAH, as shown in Figure 3.

In NOAH, the correction function of temperature depends on air temperature, T_a. In HTSVS, it is determined by foliage temperature and plant characteristics (Tab. 4). The correction functions may be slightly steeper or flatter and the temperature range of transpiration may be wider or smaller in HTSVS than in NOAH (see Fig. 3).

Both LSMs apply the same correction function to consider the limiting effects of plant available soil water (Fig. 3, Tab. 4).

In NOAH, surface skin-temperature is calculated by use of a single linearized surface energy balance equation that represents the combined soil/vegetation surface. Total evapotranspiration is the sum of the direct evaporation from the top shallow soil layer, evaporation of intercepted water and transpiration via canopy and roots (see Chen and Dudhia 2001a). A diurnally dependent Penman potential evaporation approach considers evaporation from the shallow soil layer (Mahrt and Ek 1984).

In HTSVS, the effects of bare and plant-covered soil are linearly weighted by the shielding factor σ_f ($0 \leq \sigma_f \leq 1$) associated with the degree to which foliage prevents short-wave radiation from reaching the ground (Deardorff 1978). This mixture-approach considers the microscale heterogeneity of the soil-vegetation system. As such, albedo and emissivity of canopy and soil may differ. In HTSVS, coupled energy- and water-budget equations are simultaneously solved for the surfaces of foliage and soil to calculate the corresponding surface values of temperatures and moisture (e.g., Kramm et al. 1994, 1996). The water budget equation of foliage is eliminated assuming saturation in the stomatal cavities. The water and heat fluxes of the uppermost soil layer are determined by the assumption of height-invariant fluxes (e.g., Sasamori 1970, Kramm et al. 1996). Figure 4 exemplary shows the difference of foliage and ground temperature during the diurnal course. These differences between foliage and ground temperature are neglected in NOAH that uses a common skin-temperature.

3.8. Emissivity and albedo

As a consequence of the different treatment of energy- and water budgets, the surface albedo and emissivity of NOAH and HTSVS differ (cf. Tabs. 3, 5). In NOAH, namely, albedo and emissivity are held constant throughout the entire simulation time. The albedo/emissivity of vegetation is assumed to be representative for the common albedo/emissivity of the vegetation-soil system. In general, in regions covered by snow, ground albedo and emissivity are modified based on snow depth according to Chen et al. (1997) and Koren et al. (1999).

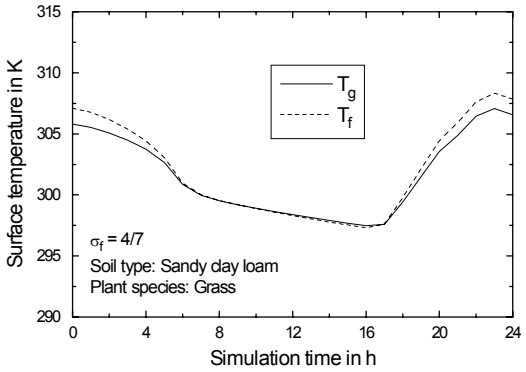

Fig. 4. Diurnal course of foliage and ground surface temperature as simulated by HTSVS.

In HTSVS, a region is assumed to be totally snow-covered after a snow event. Snow albedo and emissivity depend on snow age, t_{snow} in s, after the last snowfall (Mölders et al. 2003a).

As a consequence of the mixture approach, in HTSVS, the values of soil albedo and emissivity may differ from those of vegetation. While in HTSVS, the albedo of vegetation, α_f, is prescribed (see Tab. 5), soil albedo, α_s, depends on the volumetric water content of the uppermost shallow soil layer (McCumber and Pielke 1981).

Under snow-free conditions albedo decreases after sunset when upward soil moisture fluxes or dew feed the uppermost soil layer. In NOAH, domain averaged albedo keeps constant as long as no snow falls. A sensitivity study was performed with HTSVS wherein the albedo values of NOAH were used for the canopy. The results of this study lead to, on average, slightly higher net radiation, and latent heat fluxes, but daytime net radiation is still lower in HTSVS than in NOAH.

3.9. Roots

In NOAH, root layers follow a thin 0.05 m top layer. Roots exist up to 2 m depth. The fourth layer depth with a depth of 1 m serves as a reservoir with gravity drainage at the bottom. The soil moisture in the upper 2-m root zone is available for plant transpiration.

In HTSVS, depending on vegetation type roots may reach into all soil layers. There may be a different amount of roots in the upper 0.3 m than in the soil below (see Mölders et al. 2003a). Maximum root length may not exceed the bottom of the soil model, which is at a depth of 2 m for this study. In the upper (lower) root zone, the roots are distributed uniformly. The water extraction by roots χ is determined by Cowan's (1965) model slightly modified by Federer (1979) and Martin (1990).

3.10. Snow

NOAH uses a one-layer snow model as described in Chen et al. (1996) and Koren et al. (1999), in which snow properties are allowed to vary temporally; for example, snow density varies with snow temperature, snow melt and snow accumulation.

HTSVS applies a strongly modified version of the multi-layer snow model described by Fröhlich and Mölders (2002). Herein, snow-height, increases by snowfall and decreases by snow-metamorphism, namely (1) sublimation, (2) outflow of melt-water, and the increase of snow-density by (3) windbreak, (4) compaction, (5) settling, (6) percolation, and (7) freezing of melt-water.

4. Conclusions

Based on the few common evaluations made so far both LSMs provide the typical differences in near-surface quantities and fluxes associated with different land-use types. Predicted fluxes and skin temperature are more sensitive to the choice of LSM than the variables of state, soil temperature and soil moisture.

The comparison of the physical formulations showed that the consideration of Dufor- and Ludwig-Soret effect in the equations of heat and water transport within the soil, as well as the consideration of micro-scale heterogeneity of soil and vegetation in the energy and water budgets by HTSVS, and neglected in NOAH, are the most important differences between the two LSMs. Moreover, the realization of soil ice strongly differs. Despite these and other minor differences, the results obtained by applying these LSMs alternatively are often satisfyingly within the range of the observations (see Zhang and Tilley 2003, this volume, Mölders et al. 2003a, b). The main differences occur in the partitioning of energy between ground heat flux, and the fluxes of sensible and latent heat (see Mölders 2000).

A more generalized evaluation has to be postponed until a larger set of simulations for other synoptic situations, stations, has been performed and compared to observations.

Acknowledgments

This study was financially supported by BMBF, NSF, Johns Hopkins University under the University Partnership for Operational Support initiative, and the Geophysical Institute under contracts 07ATF30, 01 LD0036 and OPP/0002239.

References

Beringer, J., A.H. Lynch, F.S. Chapin II, and M. Mack, 2001. The representation of Arctic soils in the land surface model: The importance of mosses. *J. Climate*, **14**, 3324-3335.

Chen, F., and J. Dudhia, 2001a. Coupling an advanced land surface hydrology model with the Penn State/NCAR MM5 modeling system. Part I: Model implementation and sensitivity. *Mon. Wea. Rev*. **129**, 569-585.

Chen, F., and J. Dudhia, 2001b. Coupling an advanced land surface hydrology model with the Penn State/NCAR MM5 modeling system. Part II: Preliminary model evaluation. *Mon. Wea. Rev*. **129**, 587-604.

Chen, F., K. Mitchell, J. Schaake, Y. Xue, H.-L. Pan, V. Koren, Q.Y. Duan, M. Ek, and A. Betts, 1996. Modeling of land surface evaporation by four schemes and comparison with FIFE observations. *J. Geophys. Res*., **101D**, 7251-7268.

Chen, T.H., A. Henderson-Sellers, A.J. Pitman, Y. Shao, A. Boone, F. Chen, C.A. Desborough, K. Laval, J. Lean, D.P. Lettenmaier, X. Liang, J.-F. Mahouf, K. Mitchell, O.N. Nasonova, J. Noilhan, J. Polcher, A. Robock, A. Schlosser, J.P. Schulz, A.B. Shmakin, D.L. Verseghy, P. Welzel, E.F. Wood, Y. Xue, and Z.-L. Yang, 1997. Cabauw experimental results from the project of intercomparison of land-surface schemes (PILPS). *J. Climate* 10, 1194-1215.

Clapp, R., and G. Hornberger, 1978. Empirical equations for some soil hydraulic properties. *Water Resour. Res*., **14**, 601-604.

Colbeck, S.C., 1978. The physical aspects of water flow through snow. *Advances in hydroscience*, 165-206.

Cosby, B.J. G.M. Hornberger, R.B. Clapp, and T.R. Ginn, 1984. A statistical exploration of the relationships of soil moisture characteristics to the physical properties of soils. *Water Resour. Res*., **20**, 682-690.

Cowan, I.R., 1965. Transport of water in soil-plant-atmosphere system. *J. Appl. Ecol*., **2**, 221-239.

de Vries, D.A., 1958. Simultaneous transfer of heat and moisture in porous media. *Transactions Am. Geophys. Union*, **39**, 909-916.

Deardorff, J.W., 1978. Efficient prediction of ground surface temperature and moisture, with inclusion

of a layer of vegetation. *J. Geophys. Res*., **84C**, 1889-1903.

Dingman, S.L., 1994. *Physical Hydrology*. Macmillan Publishing Company, New York, Oxford, Singapore, Sydney, 575 pp.

Ek, M., and L. Mahrt, 1991. *OSU 1D-PBL model user's guide*. Dep. of Atmos. Sci., Oregon State Univ. Corvalis, Oregon.

Federer, C.A., 1979. A soil-plant-atmosphere model for transpiration and availability of soil water. *Water Resour. Res*., **15**, 555-562.

Fröhlich, K., and Mölders, N., 2002. Investigations on the impact of explicitly predicted snow metamorphism on the microclimate simulated by a meso-β/γ-scale non-hydrostatic model. *Atmos. Res*. 62: 71-109.

Fuchs, M., Campbell, G.S., and Papendick, R.I., 1978. An analysis of sensible and latent heat flow in partially frozen unsaturated soil. *Soil Sci. Society of America Journal*, **42**, 379-385.

Jackson, R.B., J. Canadell, J.R. Ehleringer, H.A. Mooney, O.E. Sala, and E.D. Schulze, 1996. A global analysis of root distributions for terrestrial biomes. *Oecologia*, **108**, 389-411.

Jarvis, P.G., 1976. The interpretation of the variations in leaf water potential and stomal conductance found in canopies in the field. Phil. *Trans. R. Soc. Lond. B.*, **273**, 593-610.

Koren, V., J. Schaake, K. Mitchell, Q.-Y. Duan, F. Chen, and J. M. Baker, 1999: A parameterization of snowpack and frozen ground intended for NCEP weather and climate models, *J. Geophys. Res*., **104**, 19,569-19,585.

Kramm, G., R. Dlugi, N. Mölders, and H. Müller, 1994. Numerical investigations of the dry deposition of reactive trace gases. In: Baldasano, J.M., C.A. Brebbia, H. Power, P. Zannetti (eds.), *Air Pollution II Vol. 1: Computer Simulation*, Computational Mechanics Publications, Southampton, Boston, 285-307.

Kramm, G., 1995. *Zum Austausch von Ozon und reaktiven Stickstoffverbindungen zwischen Atmosphäre und Biosphäre*. Maraun-Verlag, Frankfurt, pp. 268.

Kramm, G., N. Beier, T. Foken, H. Müller, P. Schröder, and W. Seiler, 1996. A SVAT scheme for NO, NO_2, and O_3 - model description. *Meteorol. Atmos. Phys*., **61**, 89-106.

Mahrt, L., and M. Ek, 1984. The influence of atmospheric stability on potential evaporation. *J. Clim. Appl. Meteorol*. **23**, 222-234.

Martin, P., 1990. *Forst succesion and climatic change: coupling land-surface processes and ecological dynamics*. Ph.D. Thesis NCAR/CT-131.

McCumber, M.C., and R.A. Pielke, 1981. Simulation of the effects of surface fluxes of heat and moisture in a mesoscale model, I soil layer. *J. Geophys. Res*., **86**, 9929-9938.

Mitchell, K., et al, Reducing near-surface cool/moist biases over snowpack and early spring wet soils in NCEP ETA model forecasts via land surface model upgrades, 16th conference on hydrology, Orlando, 2002.

Mölders, N., 2000. HTSVS - A new land-surface scheme for MM5. In*: The tenth PSU/NCAR Mesoscale model users' workshop,* 33-35, http://www.mmm.ucar.edu/mm5/mm5-home.html).

Mölders, N., Haferkorn, U., Döring, J., and Kramm, G., 2003a. Long-term numerical investigations on the water budget quantities predicted by the hydro-thermodynamic soil vegetation scheme (HTSVS) – Part I: Description of the model and impact of long-wave radiation, roots, snow, and soil frost. *Meteorol. Atmos. Phys*. 20pp. (in press)

Mölders, Haferkorn, U., Döring, J., and Kramm, G., 2003b. Long-term numerical investigations on the water budget quantities predicted by the hydro-thermodynamic soil vegetation scheme (HTSVS) – Part II: Evaluation, sensitivity, and uncertainty. *Meteorol. Atmos. Phys*. 20pp. (in press)

Philip, J.R., and D.A. de Vries, 1957. Moisture in porous materials under temperature gradients. *Transactions Am. Geophys. Soc*., **18**, 222-232.

Sasamori, T., 1970. A numerical study of atmospheric and soil boundary layers. *J. Atmos. Sci*., **27**, 1122-1137.

Tilley, J. S. and A. H. Lynch, 1998. On the applicability of current land surface schemes for Arctic tundra: An intercomparison study. J. Geophys. Res. 103,D22, 29051-29063.

Wilson, M.F., A. Henderson-Sellers, R.E. Dickinson, P.J. Kennedy, 1987. Sensitivity of the biosphere-atmosphere transfer scheme (BATS) to the inclusion of variable soil characteristics. *J. Clim. Appl. Met*., **26**, 341-362.

Zhang, J., and J.S. Tilley, 2001. Mesoscale simulations of cold season Alaskan atmosphere-surface interactions using PSU/NCAR MM5 model coupled to the NOAH-LSM land surface model. Sixth conference on Polar Meteorology and Oceanography. San Diego.

Zhang, J., and J.S. Tilley, 2003. Off-line tests of the land surface model NOAH-LSM for Alaskan sites. Seventh conference on polar meteorology, Boston.

Table 1. Soil profile characteristics as used in NOAH. Here, k_s, η_s, η_{fc}, η_{pwp}, b, Ψ'_s (= $-\Psi_s$) and $c_S\rho_S$ are the saturated hydraulic conductivity, porosity, field capacity, permanent wilting point, pore-size distribution index, soil water tension (= minus metric water potential) at saturation, and volumetric heat capacity of soil material. Parameters are taken from Cosby et al. (1984).

Soil type	k_s	η_s	η_{fc}	η_{pwp}	B	Ψ'_s(=-Ψ_s)
	10^{-6} m/s	m^3/m^3	m^3/m^3	m^3/m^3	-.-	m
Sand	1.07	0.339	0.236	0.01	2.79	0.069
loamy sand	1.41	0.421	0.283	0.028	4.26	0.036
sandy loam	5.23	0.434	0.312	0.047	4.74	0.141
silt loam	2.81	0.476	0.36	0.084	5.33	0.759
Silt	2.81	0.476	0.36	0.084	5.33	0.759
Loam	3.38	0.439	0.329	0.066	5.25	0.355
sandy clay loam	4.45	0.404	0.314	0.067	6.66	0.135
silty clay loam	2.04	0.464	0.387	0.12	8.72	0.617
clay loam	2.45	0.465	0.382	0.103	8.17	0.263
sandy clay	7.22	0.406	0.338	0.1	10.73	0.098
silty clay	1.34	0.468	0.404	0.126	10.39	0.324
clay	0.974	0.468	0.412	0.138	11.55	0.468
organic material	3.38	0.439	0.329	0.066	5.25	0.355
bedrock	0.0974	0.25	0.233	0.094	11.55	7.59
other (land-ice)	1.34	0.421	0.283	0.028	11.55	0.036

Table 2. Soil profile characteristics used in HTSVS. Here, k_s, η_s, b, ψ_s and $c_S\rho_S$ are the saturated hydraulic conductivity, porosity, volumetric water content at saturation, pore-size distribution index, water potential at saturation, and volumetric heat capacity of the dry soil material. Parameters are from Clapp and Hornberger (1978), Cosby et al. (1984), Pielke (1984), Chen and Dudhia (2001), and Beringer et al. (2001). In accord with Dingman (1994) field capacity and volumetric water content at permanent wilting point are the values when water potential reaches a value of -3.4m and -150m, respectively.

Soil-type	k_s 10^{-4} m/s	η_s m^3/m^3	b -.-	ψ_s m	$c_S\rho_S$ $10^6 Jm^{-3}K^{-1}$	ε_g -.-
sand	1.760	0.395	4.05	-0.121	1.47	0.95
loamy sand	1.563	0.410	4.38	-0.090	1.41	0.95
sandy loam	0.341	0.435	4.90	-0.218	1.34	0.95
silt loam	0.072	0.485	5.30	-0.786	1.27	0.95
silt	2.81	0.476	5.33	-0.759	1.27	0.95
loam	0.070	0.451	5.39	-0.478	1.21	0.95
sandy clay loam	0.063	0.420	7.12	-0.299	1.18	0.95
silty clay loam	0.017	0.477	7.75	-0.356	1.32	0.95
clay loam	0.025	0.476	8.52	-0.630	1.23	0.95
sandy clay	0.022	0.426	10.40	-0.153	1.18	0.95
silty clay	0.010	0.492	10.40	-0.490	1.15	0.95
clay	0.013	0.482	11.40	-0.405	1.09	0.95
organic material	3.38	0.451	5.25	-0.355	0.84	0.97
bedrock	0.0974	0.25	11.55	-7.59	1.9131	0.98
glaciers	1.34	0.421	11.55	-0.036	1.92556	0.82
peat	0.2	0.7	4	-0.12	1	0.97
lichen	1.5	0.9	1	-0.12	1	0.97
moos	2.0	0.95	0.5	-0.85	1	0.97

Table 3. Parameters as used in NOAH. Here, $r_{st,min}$, α, ε, z_0, R_{GL}, and h_S are the minimum stomatal resistance, the common albedo and emissivity of both foliage and ground, the roughness length as well as coefficients used in the determination of stomatal resistance, respectively.

Land-use	$r_{st,min}$	α	ε	z_0	R_{GL}	h_s
	s/m	-.-	-.-	m	Wm^{-2}	kg/kg
urban and built up land	200	0.25	0.85	1	999	999
Dryland, cropland, pasture	40	0.19	0.9	0.07	100	36.25
Irrigated cropland and pasture	40	0.15	0.9	0.07	100	36.25
mixed dryland/irrigated cropland and pasture	40	0.17	0.9	0.07	100	36.25
Cropland/grassland mosaic	40	0.19	0.9	0.07	100	36.25
Cropland/woodland mosaic	70	0.19	0.9	0.15	65	44.14
Grassland	40	0.19	0.97	0.08	100	36.35
Shrubland	300	0.25	0.95	0.03	100	42.00
mixed shrubland/grassland	170	0.23	0.95	0.05	100	39.18
Savannah	70	0.20	0.9	0.86	65	54.53
deciduous broadleaf forest	100	0.12	0.95	0.80	30	54.53
deciduous needleleaf forest	150	0.11	0.95	0.85	30	47.35
evergreen broadleaf forest	150	0.11	0.97	2.65	30	41.69
evergreen needleleaf forest	125	0.10	0.97	1.09	30	47.35
mixed forest	125	0.12	0.96	0.8	30	51.93
water bodies	-.-	0.19	0.993	0.0001	30	51.75
herbaceous wetlands	40	0.12	0.98	0.04	100	60.00
Wooded wetland	100	0.12	0.98	0.5	30	51.93
barren or sparsely vegetated	999	0.12	0.91	0.01	999	999
herbaceous tundra	150	0.16	0.97	0.04	100	42.00
Wooded tundra	150	0.16	0.97	0.06	100	42.00
mixed tundra	150	0.16	0.97	0.05	100	42.00
bare ground tundra	200	0.17	0.97	0.03	100	42.00
snow or ice	-.-	0.8	0.82	0.01	999	999

Table 4. Correction functions for stomatal resistance, $r_{st} = r_{st,min}/(\mathrm{LAI}\, g_1 g_2 g_3 g_4)$ as used in the simulations. Here, $f = 1.1\, R_s{\downarrow}/(R_{GL}\cdot \mathrm{LAI})$, $R_s{\downarrow}$ is the solar radiation, $\mathrm{PAR} = 49\sigma_f R_s{\downarrow}$ is the photosynthetic active radiation, the parameter, h_s, is given in Tab. 3, q_s and q_v are the specific humidity and that at saturation for air temperature, T_a, ρ is the density of air, δq is the water vapor deficit, $bT = (T_{max} - T_{opt})/(T_{opt} - T_{min})$, and Δz_i is the thickness of the ith soil layer.

	NOAH	HTSVS
Radiation	$g_1 = \left(\frac{r_{st,min}}{5000} + f\right) \Big/ (1+f)$	$g_1 = \frac{1}{1 + \frac{b_{st}}{PAR}}$
water vapor deficit	$g_2 = \frac{1}{1 + h_s\left(q_s(T_a) - q_v\right)}$	$g_2 = 1 + 66.6\, \rho\, \delta q$
Temperature	$g_3 = 1 - 0.0016\left(298 - T_a\right)^2$	$g_3 = \left(\frac{T_f - T_{min}}{T_{opt} - T_{min}}\right) \Big/ \left(\frac{T_{max} - T_f}{T_{max} - T_{opt}}\right)^{b_T}$
soil moisture	$g_4 = \sum_j \frac{(\eta_j - \eta_{pwp})\Delta z_j}{(\eta_{fc} - \eta_{pwp}) z_{root}}$	Same, but root depth and root distribution depend on vegetation type

Table 5. Plant specific parameters as used in HTSVS. Here, $r_{st,min}$, ψ_c, m, a, R_r, b_{st}, T_{min}, T_{max}, T_{opt}, ε_f, α_f and z_{root} are the soil water potential at which the production of cytokinis by roots is sufficiently reduced to close stomata, the fine root (ovendry) biomass, the partitioning of roots between the upper and lower root zone, the mean root radius, a parameter used to calculated stomatal resistance, the temperatures at which stomata close, the temperature at which r_{st} reaches its minimum, the albedo and emissivity of foliage, and the maximum root depth, respectively. Average volumetric density of roots (ovendry) is assumed to be equal to 500 kg/m^3. Note that if root depth exceeds the maximum depth of the soil model 2 m is assumed as maximum root depth. Parameters are taken from Pielke (1984), Wilson et al. (1987), and Jackson et al. (1996), respectively. Furthermore, z_0 is roughness length.

Land-use	$r_{st,min}$	ψ_c	m	a	R_r	b_{st}	T_{min}	T_{max}	T_{opt}	α_f	ε_f	z_{root}	z_0
	s/m	m	kg/m^2	-.-	10^{-4}m	-.-	°C	°C	°C	-.-	-.-	m	m
urban and built up land	200	-255	20	0.02	3.5	50	5	45	25	0.25	0.85	2.9	1
dryland, cropland, pasture	100	-102	20	0.5	2.51	25	5	40	24	0.19	0.9	2.1	0.07
irrigated crop., pasture	100	-102	20	0.5	2.51	25	5	40	24	0.15	0.9	2.1	0.07
mixed dryl./irri. crop. past.	100	-102	20	0.5	2.51	25	5	40	24	0.17	0.9	0.32	0.07
cropland/grassland mosaic	100	-102	20	0.5	2.51	25	5	40	24	0.19	0.9	2.35	0.07
cropland/woodland mosaic	100	-102	20	0.5	2.51	25	5	40	24	0.19	0.9	2.82	0.15
Grassland	70	-92	70	0.24	0.925	20	5	45	9	0.19	0.97	2.6	0.08
Shrubland	300	-133	4.8	0.36	2.51	10	5	45	25	0.25	0.95	7.0	0.03
mixed shrubland/grassland	70	-133	4.9	0.36	2.51	10	5	45	25	0.23	0.95	4.8	0.05
Savannah	70	-92	5.4	0.24	0.925	20	5	45	9	0.20	0.9	15.0	0.86
deciduous broadleaf forest	100	-214	1.2	0.02	3.5	22	10	45	25	0.12	0.95	3.7	0.80
deciduous needleleaf forest	232	-214	7.1	0.02	3.5	22	10	45	25	0.11	0.95	2.9	0.85
evergreen broadleaf forest	150	-163	4.9	0.16	3.5	25	-5	35	25	0.11	0.97	3.7	2.65
evergreen needleleaf forest	125	-163	12.7	0.02	3.5	25	-5	35	25	0.10	0.97	3.9	1.09
mixed forest	125	-158	8.2	0.02	3.5	23	0	40	25	0.12	0.96	3.12	0.8
water bodies	-.-	-.-	-.-	-.-	-.-	-.-	-.-	-.-	-.-	0.19	0.993	-.-	0.0001
herbaceous wetlands	40	-92	70	0.36	0.925	20	5	45	9	0.12	0.98	0.5	0.04
wooded wetland	100	-163	15.3	0.02	3.5	20	5	45	9	0.12	0.98	1.81	0.5
bare or sparsely vegetated	999	-92	3.3	0.22	0.925	20	5	45	9	0.12	0.91	0.5	0.01
herbaceous tundra	150	-92	10.8	0.4	2.51	20	5	45	9	0.16	0.97	0.5	0.04
wooded tundra	150	-163	15.5	0.4	3.5	40	5	40	25	0.16	0.97	1.81	0.06
mixed tundra	150	-163	2.9	0.4	3.5	40	5	40	25	0.16	0.97	1.81	0.05
bare ground tundra	200	-163	10.8	0.4	0.925	40	5	40	25	0.17	0.97	0.5	0.03
snow or ice	-.-	-.-	-.-	-.-	-.-	-.-	-.-	-.-	-.-	0.8	0.82	-.-	0.01